

# 光学学报

## 变温环境下谐振式光纤陀螺偏振误差研究

高天香<sup>1</sup>, 李俊<sup>2</sup>, 蓝士祺<sup>2</sup>, 吴凡<sup>2</sup>, 程峻<sup>1</sup>, 齐新元<sup>1\*</sup>

<sup>1</sup>西北大学物理学院, 陕西 西安 710127;

<sup>2</sup>西安飞行自动控制研究所飞行器控制一体化技术国防科技重点实验室, 陕西 西安 710076

**摘要** 偏振噪声是谐振式光纤陀螺谐振腔中较为严重的光学噪声之一。基于琼斯矩阵的方法建立完整的光路传输模型, 对谐振腔顺时针和逆时针两路光传输进行分析, 得到环境温度在−40℃~80℃范围内变化时偏振噪声导致的陀螺误差。结果表明, 在线起偏器消光比为30 dB时, 耦合器直通端对准角度误差小于2.78°, 耦合系数为0.05, 双90°熔接点两侧光纤长度差容错值在0.207 m以内, 使得陀螺输出误差小于0.01(°)/h。基于此, 当陀螺系统工作导致内部温度分布非均匀时, 谐振腔上每相邻两段光纤间温度分布差需小于3.122℃。各影响因素的参数选择可为变温环境下由于偏振噪声导致的误差分配设计提供理论指导。

**关键词** 谐振式光纤陀螺; 琼斯矩阵; 偏振噪声; 变温环境

中图分类号 V241.5+9

文献标志码 A

DOI: 10.3788/AOS230635

### 1 引言

谐振式光纤陀螺(RFOG)是新型的光学陀螺之一, 其利用Sagnac效应<sup>[1-3]</sup>测量载体的角速度信息。RFOG具有理论精度高、无锁区、动态范围大等优点<sup>[4-6]</sup>, 受到众多科研院所和高校的关注及研究。

偏振噪声是导致RFOG输出存在误差的主要光学噪声之一<sup>[6-10]</sup>。由于其核心敏感部件光纤环形谐振腔(FRR)多由保偏光纤绕制而成, 保偏光纤的双折射率随温度变化时, 会导致FRR的两个本征偏振态(ESOP)各自所对应的谐振光波发生叠加与干涉, 引起谐振曲线的不对称, 从而导致谐振频率点的检测误差, 进而引起陀螺输出误差, 这是形成偏振噪声的主要原因。研究人员为抑制偏振噪声采取的措施可分为稳定主次偏振相位差和减小次偏振态强度两类。在稳定主次偏振相位差方面, 研究人员通过对保偏光纤谐振腔中的偏振特性进行研究<sup>[10]</sup>, 先后采用FRR内单点90°熔接方案<sup>[10]</sup>及双90°熔接保偏透射FRR方案<sup>[11]</sup>, 在此基础上, 设计两次偏振轴旋转熔接起偏谐振腔<sup>[12-13]</sup>, 大幅改善了FRR偏振稳定性。在减小次偏振态强度方面, 研究人员通过在FRR内插入偏振控制器<sup>[14]</sup>、在线起偏器<sup>[13]</sup>等使次偏振态大幅衰减, 或者利用单偏振光纤<sup>[15]</sup>、本征偏振态对温度敏感性更低的空芯光子晶体带隙光纤<sup>[16]</sup>、空芯光子晶体光纤结合偏振分束器<sup>[17]</sup>、无节点抗谐振光纤<sup>[18]</sup>等新型光纤方案降低偏振噪声对陀螺的影响。以上研究有较好的噪声

抑制效果, 使次偏振态得到抑制或两个偏振态的相位差稳定, 大大减少了外界温度变化引起的偏振噪声, 但多数研究都是在常温或者小范围变温情况下进行的。而陀螺面向工程化应用时需要在全温范围内提高环境适应性, 目前对RFOG的研究难以兼顾高精度和工程化应用两方面的需求, 在变温环境下对影响偏振噪声从而影响陀螺输出误差的研究较少, 且系统实际构成和理论计算之间存在差距, 导致误差抑制的效果不够好。

本文基于琼斯矩阵的方法建立完整光路传输模型, 对谐振腔顺时针和逆时针两路光传输进行分析, 将顺、逆时针偏振模式耦合误差的差值作为陀螺输出误差。在全温范围−40℃~80℃内仿真计算耦合器直通端角度对准误差、双90°熔接点两侧光纤长度差、系统内局部升温时FRR上非均匀温度分布差等因素对偏振噪声的影响及这些影响如何作用到陀螺输出误差, 并在变温环境下针对特定的陀螺误差需求对以上参数的控制精度进行具体数值量化。

### 2 建模仿真分析

#### 2.1 谐振腔光路建模

透射式光纤环形谐振腔结构如图1所示, 腔内包含2个耦合器C<sub>1</sub>、C<sub>2</sub>, 4段光纤L<sub>1</sub>、L<sub>2</sub>、L<sub>3</sub>、L<sub>4</sub>, 慢轴在线起偏器P<sub>x</sub>和快轴在线起偏器P<sub>y</sub>(分别对谐振腔内快轴传输方向和慢轴传输方向的偏振态造成大的衰减), 以及2个90°熔接点, 交叉号表示熔接点位置。

收稿日期: 2023-03-07; 修回日期: 2023-04-14; 录用日期: 2023-05-05; 网络首发日期: 2023-05-15

通信作者: \*qixycn@nwu.edu.cn

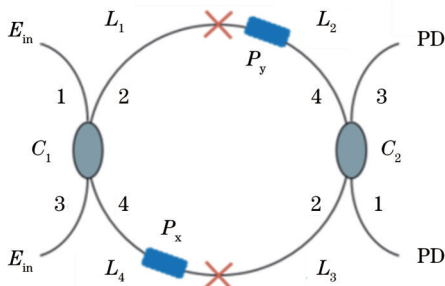


图1 集成在线起偏器的光纤环形谐振腔

Fig. 1 FRR with in-line polarizers

琼斯矩阵是一种描述光学器件偏振特性的简单方法,本文将基于此方法分别分析顺时针(CW)和逆时针(CCW)光传输的偏振特性。

耦合器 $C_i(i=1,2)$ 的4端口到2端口或3端口到1端口为直通端,其琼斯矩阵为

$$\begin{cases} T_{z_{\text{CW}i}} = \sqrt{1-k} \begin{pmatrix} \cos \theta_{zi} & -\sin \theta_{zi} \\ \sin \theta_{zi} & \cos \theta_{zi} \end{pmatrix}, \\ T_{z_{\text{CCW}i}} = \sqrt{1-k} \begin{pmatrix} \cos \theta_{zi} & \sin \theta_{zi} \\ -\sin \theta_{zi} & \cos \theta_{zi} \end{pmatrix}, \end{cases} \quad (1)$$

式中:下标*i*可取1或2,表示两个不同的耦合器; $\theta_{zi}$ 表示耦合器直通端等效角度对准误差; $k$ 是耦合器耦合系数。

耦合器 $C_i(i=1,2)$ 的1端口到4端口或3端口到2端口为交叉端,其琼斯矩阵为

$$\begin{cases} T_{r_{\text{CW}i}} = \sqrt{k} \begin{pmatrix} \cos \theta_{ri} & -\sin \theta_{ri} \\ \sin \theta_{ri} & \cos \theta_{ri} \end{pmatrix}, \\ T_{r_{\text{CCW}i}} = \sqrt{k} \begin{pmatrix} \cos \theta_{ri} & \sin \theta_{ri} \\ -\sin \theta_{ri} & \cos \theta_{ri} \end{pmatrix}, \end{cases} \quad (2)$$

式中: $\theta_{ri}$ 表示耦合器交叉端等效角度对准误差。

每段光纤的传输矩阵 $S_i(i=1,2,3,4)$ 的表达式为

$$S_i = \begin{pmatrix} \exp(-j\beta_x L_i) & 0 \\ 0 & \exp(-j\beta_y L_i) \end{pmatrix}, \quad (3)$$

$$\begin{cases} \beta_x = 2\pi \frac{n_x}{\lambda} \\ \beta_y = 2\pi \frac{n_y}{\lambda} \end{cases}, \quad (4)$$

式中: $\beta_x$ 和 $\beta_y$ 分别是慢轴和快轴的传输常数; $n_x, n_y$ 分别是保偏光纤慢轴和快轴的折射率; $\lambda$ 是中心波长,为1550 nm。

在线起偏器 $P_x, P_y$ 的传输矩阵为

$$\begin{cases} P_x = \begin{pmatrix} 1 & 0 \\ 0 & \delta_x \end{pmatrix} \\ P_y = \begin{pmatrix} \delta_y & 0 \\ 0 & 1 \end{pmatrix} \end{cases}, \quad (5)$$

式中: $\delta_x$ 和 $\delta_y$ 分别是慢轴和快轴在线起偏器的消光比。

熔接点顺逆时针传输矩阵分别为

$$\begin{cases} R_{\text{CW}} = \begin{pmatrix} \cos \theta & -\sin \theta \\ \sin \theta & \cos \theta \end{pmatrix} \\ R_{\text{CCW}} = \begin{pmatrix} \cos \theta & \sin \theta \\ -\sin \theta & \cos \theta \end{pmatrix} \end{cases}, \quad (6)$$

式中: $\theta$ 是光纤熔接对准角度。

则光沿顺逆时针传输矩阵分别为

$$\begin{cases} H_{\text{CW}} = \alpha T_{z_{\text{CW}1}} S_4 P_x R_{\text{CW}} S_3 T_{z_{\text{CW}2}} S_2 P_y R_{\text{CW}} S_1 \\ H_{\text{CCW}} = \alpha T_{z_{\text{CCW}1}} S_1 R_{\text{CCW}} P_y S_2 T_{z_{\text{CCW}2}} S_3 R_{\text{CCW}} P_x S_4 \end{cases}, \quad (7)$$

式中: $\alpha$ 为光在谐振腔内传输一周的损耗。

假设输入光为线偏振光 $E_{\text{in}} = \begin{pmatrix} 1 \\ 0 \end{pmatrix}$ ,则从耦合器 $C_1$

的2端口出射的光场为 $E_{12}$ ,将光投影到两个ESOPs上:

$$E_{12} = T_{r_{\text{CW}1}} E_{\text{in}} = a \nu_{1_{\text{CW}}} + b \nu_{2_{\text{CW}}}, \quad (8)$$

式中: $\nu_{1_{\text{CW}}}$ 和 $\nu_{2_{\text{CW}}}$ 分别是两个本征偏振态; $a, b$ 代表幅度。2个ESOPs在FRR中传播*n*圈后:

$$\begin{cases} G_{E1,12} = a \nu_{1_{\text{CW}}} \sum_n \lambda_{1_{\text{CW}}}^n \\ G_{E2,12} = b \nu_{2_{\text{CW}}} \sum_n \lambda_{2_{\text{CW}}}^n \end{cases}, \quad (9)$$

式中: $\lambda_{1_{\text{CW}}}$ 和 $\lambda_{2_{\text{CW}}}$ 分别是两个本征偏振态的本征值,表示在FRR内传输一周的传输系数。2个ESOPs在 $C_2$ 的1端口出射时光场为

$$\begin{cases} G_{E1,21} = T_{r_{\text{CW}2}} S_2 P_y R_{\text{CW}} S_1 G_{E1,12} \\ G_{E2,21} = T_{r_{\text{CW}2}} S_2 P_y R_{\text{CW}} S_1 G_{E2,12} \end{cases}. \quad (10)$$

逆时针光传输同理,2个ESOPs在 $C_2$ 的3端口出射时光场为

$$\begin{cases} G_{E1,23} = T_{r_{\text{CCW}1}} S_3 R_{\text{CCW}} P_x S_4 G_{E1,14} \\ G_{E2,23} = T_{r_{\text{CCW}1}} S_3 R_{\text{CCW}} P_x S_4 G_{E2,14} \end{cases}. \quad (11)$$

## 2.2 谐振腔偏振特性分析

根据相关研究<sup>[13]</sup>可知,双90°集成在线起偏器对偏振波动的抑制效果最好,在此基础上,根据式(10)、(11),光在腔内传输一周的谐振曲线如图2所示。图2(a)为CW光的ESOPs;图2(b)为CW光多圈传输后的谐振曲线,其中,实线代表CW-ESOP1,虚线代表CW-ESOP2;图2(c)为CCW光的ESOPs;图2(d)为CCW光多圈传输后的谐振曲线,其中,点线代表CCW-ESOP1,点划线代表CCW-ESOP2。

图2(a)、(c)分别为双90°熔接集成在线起偏器结构下顺时针和逆时针传输光的ESOPs,两个偏振态接近正交,当主偏振态处于谐振工作状态时,次偏振态被极大抑制,从而使得次偏振态对主偏振态谐振曲线的影响降低,进而抑制偏振波动噪声。图2(b)、(d)分别为顺时针和逆时针的多圈传输谐振曲线,次偏振态相较于主偏振态抑制比均可达36 dB。

顺逆时针方向光电探测器探测到的光强分别为

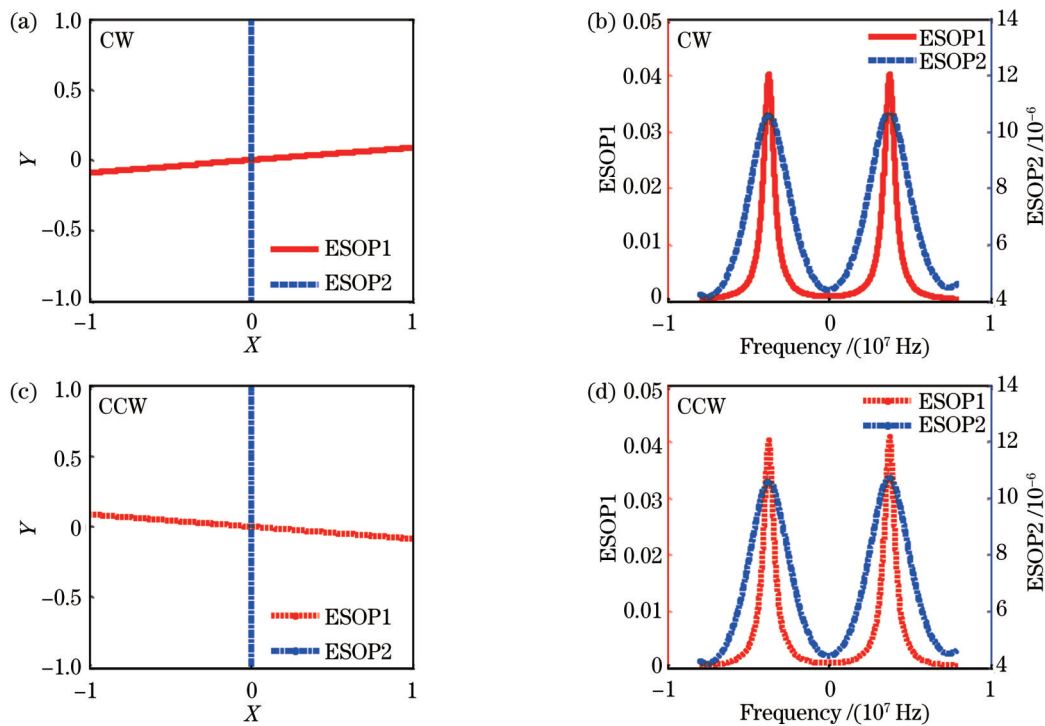


图 2 双 90°熔接保偏光纤环形谐振腔谐振曲线。(a)顺时针光ESOPs;(b)顺时针光多圈传输后谐振曲线;(c)逆时针光ESOPs;(d)逆时针光多圈传输后谐振曲线

Fig. 2 The resonant curves of FRR with twin 90° spliced polarization maintaining fiber. (a) ESOPs of CW; (b) CW resonance curve after multi-turn transmission; (c) ESOPs of CCW; (d) CCW resonance curve after multi-turn transmission

$$\begin{cases} I_{\text{CW}} = [G_{E1,21}^H + G_{E2,21}^H][G_{E1,21} + G_{E2,21}] = I_1 + I_2 + 2\text{Re}[I_3] \\ I_{\text{CCW}} = [G_{E1,23}^H + G_{E2,23}^H][G_{E1,23} + G_{E2,23}] = I'_1 + I'_2 + 2\text{Re}[I'_3], \end{cases} \quad (12)$$

式中:上标<sup>H</sup>表示共轭转置;Re[·]表示取实部; $I_1$ 和 $I_2$ 、 $I'_1$ 和 $I'_2$ 分别表示顺、逆时针ESOP1和ESOP2的强度; $I_3$ 和 $I'_3$ 表示干涉项。如果将ESOP1视为主偏振态,则ESOP2为次偏振态的强度噪声, $I_3$ 和 $I'_3$ 是干涉项噪声。顺逆时针的谐振频率偏移可以从下式求解:

$$\begin{cases} \frac{\partial I_{\text{CW}}}{\partial f} \Big|_{f=\Delta f_{\text{cw}}} = 0 \\ \frac{\partial I_{\text{CCW}}}{\partial f} \Big|_{f=\Delta f_{\text{ccw}}} = 0 \end{cases}, \quad (13)$$

式中: $\Delta f_{\text{cw}}$ 是顺时针方向偏振噪声产生的频偏; $\Delta f_{\text{ccw}}$ 是逆时针方向偏振噪声产生的频偏。在以往的计算中,常将 $2\Delta f_{\text{cw}}$ 作为陀螺系统整体偏振产生的频偏,忽略了顺逆两路光传输的差异。为消除共模误差,本研究中顺逆时针产生的频差为

$$\Delta f = \Delta f_{\text{cw}} - \Delta f_{\text{ccw}}. \quad (14)$$

陀螺输出与频差的关系为

$$\Omega_{\text{error}} = \frac{n\lambda}{d} \Delta f. \quad (15)$$

根据以上分析讨论环境温度变化时偏振噪声导致的陀螺输出误差。

### 3 变温环境下偏振噪声导致的陀螺输出误差

随着光纤陀螺工程化技术的不断发展,陀螺的环境适应性成为现阶段影响陀螺应用的主要问题,其中,温度问题最为突出,因此对陀螺偏振输出误差在全温环境下如何变化的研究尤为重要。

以双 90°集成在线起偏器的 FRR 结构为基础,研究在变温环境下偏振误差对陀螺输出的影响。参考现有实验中谐振腔的参数,本研究相关参数设置如下: $L_1$  和  $L_3$ 、 $L_2$  和  $L_4$  分别为耦合器  $C_1$ 、 $C_2$  的尾纤, $L_1$ 、 $L_2$ 、 $L_3$ 、 $L_4$  的长度分别为 6.86、6.89、7.03、6.94 m, 直径  $d$  为 0.065 m,  $P_x$  和  $P_y$  选择标称 30 dB 慢轴在线起偏器和快轴在线起偏器, 耦合器直通端角度对准误差  $\theta_{zi}$  为 5°, 交叉端角度对准误差  $\theta_{ri}$  为 6°。

由于光纤的折射率会随温度变化,因此在变温环境中,折射率的变化会导致偏振态变化从而产生偏振误差。假设保偏光纤折射率温度系数  $\frac{dn}{dT} = 1.1 \times 10^{-5} \text{ }^{\circ}\text{C}^{-1}$ , 根据前面的分析及式(1)~(15)可知,当环境温度在  $-40 \text{ }^{\circ}\text{C}$ ~ $80 \text{ }^{\circ}\text{C}$  之间时, 偏振噪声产生的误差随温度变化的关系如图 3 所示。

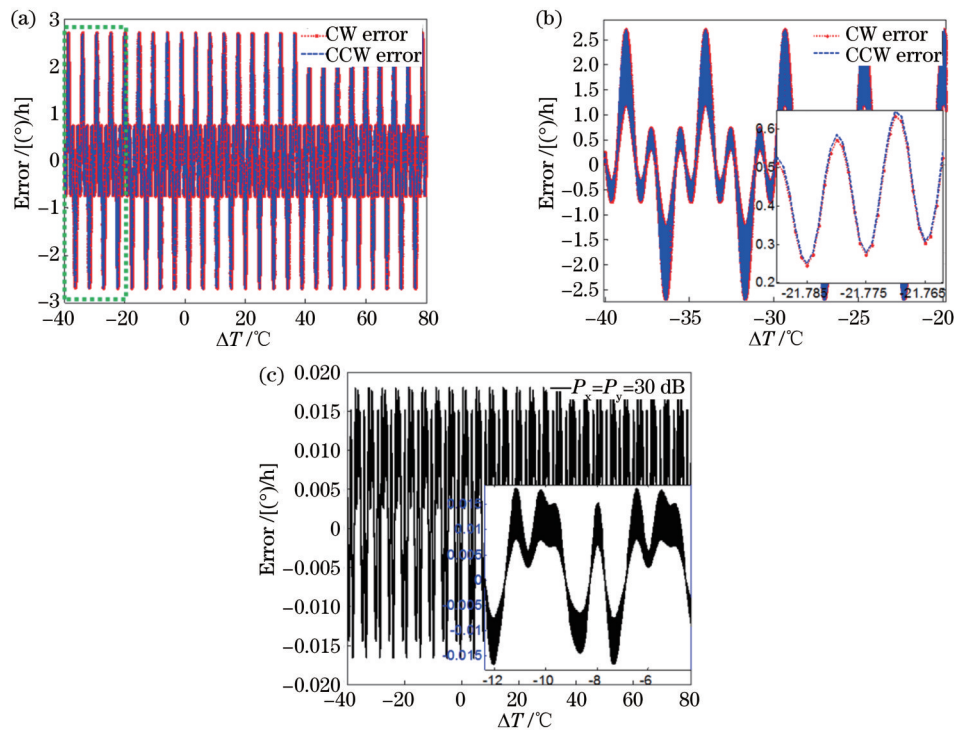


图3 双90°熔接结构在变温环境下偏振噪声导致的陀螺输出误差。(a)顺逆时针输出误差;(b)局部放大图;(c)顺逆时针输出误差差值

Fig. 3 Gyroscope output error caused by polarization noise of twin 90° spliced structure under varying temperature environment.  
(a) Output error of CW and CCW; (b) partial enlarged detail; (c) output error difference of CW and CCW

由图3(a)可知,当环境温度在全温范围内变化时,顺时针与逆时针光传输偏振导致的误差非常接近,均在 $\pm 3 (^{\circ})/\text{h}$ 之内变化,且呈现周期性变化。为更好表现其规律性,以 $-40 ^{\circ}\text{C} \sim -20 ^{\circ}\text{C}$ 为例说明,具体如图3(b)所示,从局部放大图可以清晰地看到,顺逆时针输出误差的周期相同,均为 $4.69 ^{\circ}\text{C}$ ,且数值相差很小。与以往将一路误差输出作为陀螺输出误差不同,这里以顺时针与逆时针的误差输出差值作为陀螺输出误差,消除了顺逆时针之间的共模误差,如图3(c)所示,其差值整体在 $\pm 0.2 (^{\circ})/\text{h}$ 之内,随温度而周期性变化。但是这个结果无法支撑导航级陀螺工程样机研制需求,需要通过控制其他参数降低偏振误差输出。为了研究简便,下面的讨论选取 $-40 ^{\circ}\text{C} \sim -20 ^{\circ}\text{C}$ 温度范围代替全温范围,不影响对结果判断的准确性。

#### 4 变温环境陀螺输出误差影响因素分析

作为RFOG系统的核心敏感器件FRR,其性能的好坏直接影响噪声大小。从式(1)~(12)可以看出,FRR的主要影响因素包括在线起偏器消光比、耦合器对准角度误差、双90°熔接点两侧光纤长度差,以及变温环境下FRR温度分布不均匀带来的误差。其中,影响最大的因素为在线起偏器消光比,消光比越大,FRR的偏振噪声越小<sup>[12]</sup>。目前市场成熟货架产品一般以30 dB型号居多,基于此,分别仿真计算各个因素

对陀螺输出误差的影响,并进行具体数值量化。

##### 4.1 耦合器角度对准误差对陀螺输出误差的影响

在绕制FRR时,耦合器的性能对FRR的参数影响非常大。耦合器直通端或交叉端的角度对准误差对传输光的偏振串扰影响无法忽略,这一影响最终会体现在陀螺输出误差上。因此,需要对耦合器直通端或交叉端角度对准误差进行具体数值量化。当温度范围为 $-40 ^{\circ}\text{C} \sim -20 ^{\circ}\text{C}$ 时,以耦合器直通端角度对准误差为例,其对陀螺输出误差的影响如图4所示。

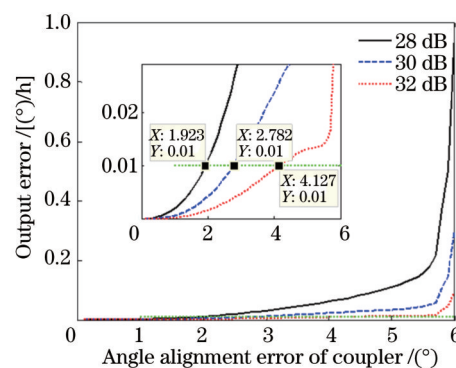


图4 在线起偏器消光比不同时耦合器直通端角度对准误差导致的陀螺输出误差

Fig. 4 Gyroscope output error caused by direct angle alignment error at the straight end of the coupler with different in-line polarizer extinction ratio

图4中实线、虚线、点线分别对应在线起偏器为28 dB、30 dB、32 dB时,耦合器直通端角度对准误差导致的陀螺输出误差。可以发现,当环境温度变化时,顺逆时针偏振导致的陀螺输出误差随着耦合器直通端角度对准误差增大而增大,但其影响小于在线起偏器消光比引起的陀螺输出误差变化量,在线起偏器消光比越大,陀螺输出误差增大趋势越缓慢。当在线起偏器消光比为30 dB,耦合器的角度对准误差小于2.78°,偏振噪声导致陀螺输出误差为0.01(°)/h。

#### 4.2 光纤长度差对陀螺输出误差的影响

由保偏光纤制作的FRR,双90°熔接点两侧的光纤长度差( $\Delta L$ )是一个较为可控的因素,如果 $\Delta L$ 不为0,会影响顺逆两束光传输的互易性,从而影响光传输偏振态,最终影响陀螺输出。选择在线起偏器消光比为30 dB,当环境温度在全温范围内变化时,不同长度差导致的陀螺输出误差也不同,而且耦合器的耦合系数也会有所影响,具体如图5所示。

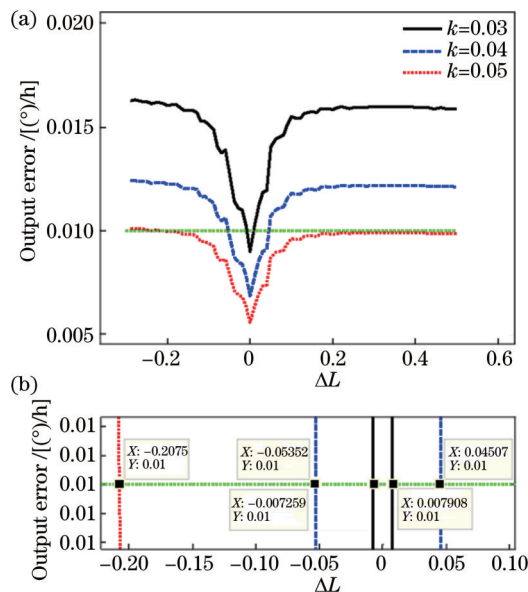


图5 光纤长度差与陀螺输出误差。(a)光纤长度差与陀螺输出误差的关系;(b)局部放大图

Fig. 5 Relationship between the  $\Delta L$  and the output error of gyroscope. (a) Relationship between the  $\Delta L$  and the output error of gyroscope; (b) partial enlarged detail

从图5(a)可以看出,当环境温度在全温范围内变化时,双90°熔接点两侧的光纤长度差越大,偏振误差越大,总体呈现增大的趋势,在长度差为0 m处陀螺偏振误差最小。这是由于在FRR结构中,90°偏振轴旋转熔接使得双折射相互抵消,腔长对于光传输的影响由 $L$ 改变为 $\Delta L$ ,使得FRR的温度稳定性提高了 $\Delta L/L$ 倍。这表明在绕制FRR时,应使腔长尽量对称,误差控制在一定长度以内,可以提高光路互易性,有利于抑制偏振噪声。

同时,耦合器的耦合系数 $k$ 越大,腔内的有效光强

越大,Sagnac效应增强,所受温度影响降低,同样的全温范围内可以达到更优的精度。图5(b)中, $k=0.03$ 、光纤长度差控制在±0.007 m以内时,偏振误差输出为0.01(°)/h,这对实际操作是一个很大的挑战。 $k=0.04$ 时,光纤长度差在-0.053~0.045 m以内。 $k=0.05$ 时,光纤长度差控制在0.207 m以内即可,大大提高了实际操作的容错值。因此在制作FRR时, $k=0.05$ 的耦合器使得尾纤长度更加可控。

#### 4.3 光纤环温度分布研究

在陀螺使用环境中,激光器或电路元件在正常工作时存在散热的问题,相比大环境温度变化,与它们距离较近的FRR会受到局部的温度扰动,这对于温度敏感的保偏光纤来说影响是严重的,因此有必要分析光纤环温度分布对陀螺偏振输出误差的影响。

##### 4.3.1 不同位置温度扰动时陀螺输出误差

根据第3.1和3.2节的分析,选择30 dB耦合器,耦合器 $k=0.05$ ,角度对准误差为2.7°,假设温度扰动分别作用在FRR的 $L_1$ 、 $L_2$ 、 $L_3$ 、 $L_4$ 上,使 $L_i$ ( $i=1,2,3,4$ )段保偏光纤折射率温度系数为 $\frac{dn(i)}{dT}=2.2 \times 10^{-5} \text{ }^{\circ}\text{C}^{-1}$ ,其他段光纤受环境温度影响不变,变温环境下陀螺输出误差结果如图6所示。

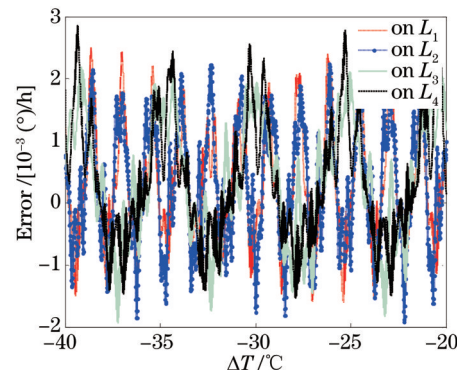


图6 优化参数选择后温度扰动作用于 $L_1$ 、 $L_2$ 、 $L_3$ 、 $L_4$ 时在变温环境下偏振噪声导致的陀螺输出误差

Fig. 6 Gyroscope output error caused by polarization noise under varying temperature environment when temperature disturbance acts on  $L_1$ ,  $L_2$ ,  $L_3$  and  $L_4$  after optimizing parameters

图6点线、点划线、实线、虚线分别表示在 $L_1$ 、 $L_2$ 、 $L_3$ 、 $L_4$ 等4段光纤上单独施加温度扰动的结果,可以看出,当环境温度从-40 °C增加到-20 °C时,不论温度扰动施加在哪一段光纤,陀螺输出误差范围均在-0.002(°)/h~0.003(°)/h以内,说明此时温度扰动对陀螺偏振输出误差的影响被极大抑制。但在实际应用场景中,温度扰动不是一个固定不变的温度扰动点,而是局部温度变化会导致FRR上温度分布非均匀,因此对温度分布的研究至关重要。

### 4.3.2 非均匀温度分布陀螺输出误差

由温度引起FRR的输出误差主要表现在两方面：1)与FRR的温度梯度即温度的时间导数成正比的Shupe误差，2)由与温度绝对值成正比的热应力导致的零偏<sup>[19-20]</sup>。一般认为，只要温度梯度随时间变化率趋于零，即温度均匀变化或变化到一个定值，Shupe误差就为零<sup>[21]</sup>。

由于FRR存在轴向空间分布，激光器或电路元件等有源器件一般在FRR下层，靠近FRR底部，陀螺系统工作时有源器件散热会导致FRR上的温度呈现非均匀分布状态，与环境温度出现差值，将这个差值称为非均匀温度分布差。当温度分布不均匀时，光纤中双折射率发生变化，使得光波在光纤中传输过程中造成一定的传输光程差，而这种差异在整段光纤长度上积分，引起热致非互易性误差，最终形成偏振噪声并作用到陀螺系统从而产生输出误差。在全温环境下，首先假设内部升温导致温度只在FRR某一段光纤上非均匀分布，以在L<sub>1</sub>段光纤上为例，不考虑热应力影响，仿真计算非均匀温度分布差与陀螺输出误差的关系，如图7所示。

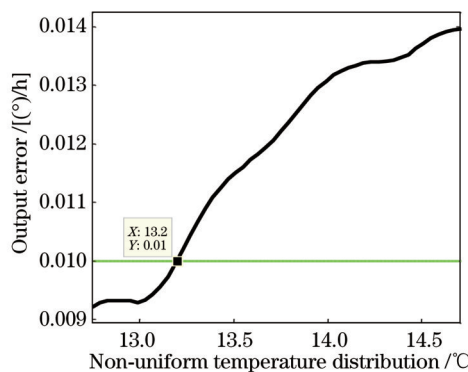


图7 L<sub>1</sub>光纤上非均匀温度分布差与陀螺输出误差的关系  
Fig. 7 Relationship between the non-uniform temperature distribution and the output error of gyroscope on L<sub>1</sub>

从图7可以看出，当温度非均匀只作用在L<sub>1</sub>段光纤上，其温度与环境温度分布差小于13.2 °C时，偏振误差项导致的陀螺输出小于0.01 (°)/h。这是由于FRR中某段光纤温度非均匀分布时，温度变化导致光纤折射率随之发生改变，两束反向传播的光波经过这段光纤时将产生一个非互易误差，形成偏振噪声，并作用到陀螺输出。

如果内部升温使得FRR每一段光纤上温度非均匀分布，以环境温度为基值，离热源越近温度差越大，离热源越远温度差越小，不考虑热应力影响，则每相邻两段光纤之间温度非均匀分布差与陀螺输出误差的关系如图8所示。

从图8可以看出，当环境温度在全温范围内变化、FRR上每两两相邻两段光纤温度非均匀分布差值小

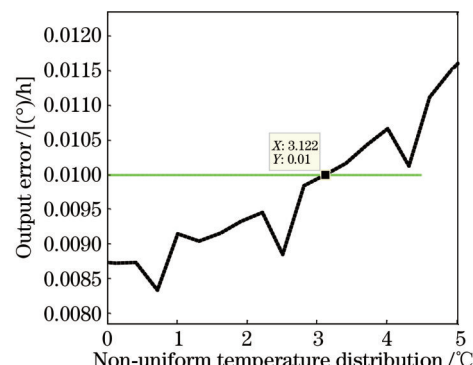


图8 每段光纤温度非均匀分布差与陀螺输出误差的关系  
Fig. 8 Relationship between the non-uniform temperature distribution and the output error of gyroscope on each segment of fiber

于3.122 °C时，偏振误差导致的陀螺输出小于0.01 (°)/h。与温度非均匀只作用在L<sub>1</sub>段光纤上时相比，两束反向传播的光波经过整段光纤时产生的非互易误差增大，达到相同的陀螺输出误差时允许温度非均匀分布差值的范围更小，因此对于器件温控及达到热平衡状态的控制手段提出更高的要求。

## 5 结 论

基于琼斯矩阵，建立FRR完整光路传输模型，通过对CW和CCW两路光传输偏振噪声进行分析，基于双点90°熔接集成在线起偏器结构，推导FRR中谐振曲线，得到变温环境下偏振误差导致的陀螺输出。由于全温范围内陀螺输出具有一定的周期性和规律性，以-40 °C~ -20 °C变温范围代替全温环境，分别对不同影响因素进行分析。结果表明，在线起偏器选择成熟货架产品30 dB消光比时，耦合器角度对准误差小于2.78°，陀螺偏振输出误差小于0.01 (°)/h。耦合器系数k越大，双90°熔接点两侧的ΔL容错值越高，k为货架产品常见的0.05、ΔL控制在0.207 m时，陀螺偏振输出误差小于0.01 (°)/h。在此基础上，考虑工程应用中陀螺样机由于内部升温导致的一段光纤上的温度非均匀分布，温度非均匀分布差需小于13.2 °C。而当FRR上每两两相邻光纤之间存在非均匀分布温度差时，其值应小于3.122 °C，这时陀螺输出误差小于0.01 (°)/h。以上分析基于陀螺偏振噪声抑制的要求，可为全温环境下误差分配设计提供一定的理论指导。需要注意的是，本研究中重点考虑温度在FRR上非均匀分布的影响，而只要FRR的温度发生变化，热应力效应引起的偏置误差就不为零，这一问题还有待继续研究。

## 参 考 文 献

- [1] Arditty H J, Lefèvre H C. Sagnac effect in fiber gyroscopes[J]. Optics Letters, 1981, 6(8): 401-403.
- [2] Ma H L, Zhang J J, Wang L L, et al. Development and

- evaluation of optical passive resonant gyroscopes[J]. Journal of Lightwave Technology, 2017, 35(16): 3546-3554.
- [3] Pan Z W, Zhang C F, Xie C F, et al. Resonator integrated optic gyro based on multilevel laser frequency lock-in technique[J]. Chinese Optics Letters, 2018, 16(4): 040601.
- [4] Sanders G A, Strandjord L K, Williams W, et al. Improvements to signal processing and component miniaturization of compact resonator fiber optic gyroscopes[C]// 2018 DGDN Inertial Sensors and Systems (ISS), September 11-12, 2018, Braunschweig, Germany. New York: IEEE Press, 2018.
- [5] Yang Y H, Yang F L. High performance fiber optic gyroscope with a radiation-tolerant and temperature-stable scale factor[J]. Chinese Optics Letters, 2016, 14(11): 110605-110609.
- [6] Shang K J, Lei M, Fang Y A, et al. Resonator fiber-optic gyro with intensity error suppression using a bias-sampling compensation technique[J]. Applied Optics, 2020, 59(13): 3995-3999.
- [7] 刘霜, 李汉钊, 刘路, 等. 激光器频率噪声功率谱密度测试技术及在谐振式光纤陀螺中的应用[J]. 光学学报, 2021, 41(13): 1306010.
- Liu S, Li H Z, Liu L, et al. Laser frequency noise power spectral density measurement technology and its application to resonant optical fiber gyroscope[J]. Acta Optica Sinica, 2021, 41(13): 1306010.
- [8] 李汉钊, 钱伟文, 刘路, 等. 谐振式光纤陀螺角度随机游走的分析与优化[J]. 中国激光, 2021, 48(9): 0901002.
- Li H Z, Qian W W, Liu L, et al. Analysis and optimization of angle random walk of resonant fiber optic gyroscope[J]. Chinese Journal of Lasers, 2021, 48(9): 0901002.
- [9] 顾帅, 皮鹏程, 廉正刚, 等. 面向光纤陀螺发展需求的空芯微结构光纤的弯曲特性研究[J]. 中国激光, 2023, 50(6): 1306002.
- Gu S, Pi P C, Lian Z G, et al. Research on bending characteristics of hollow-core micro-structured fibers for development of fiber optic gyroscopes[J]. Chinese Journal of Lasers, 2023, 50(6): 1306002.
- [10] Sanders G A, Smith R B, Rouse G F. Novel polarization-rotating fiber resonator for rotation sensing applications[J]. Proceedings of SPIE, 1990, 1169: 373-381.
- [11] Wang X J, He Z Y, Hotate K. Polarization-noise suppression by twice 90° polarization-axis rotated splicing in resonator fiber optic gyroscope[C]// Conference on Lasers and Electro-Optics/ International Quantum Electronics Conference, May 31-June 5, 2009, Baltimore, Maryland. Washington, D. C.: Optica Publishing Group, 2009: CMG1.
- [12] Wang X J, He Z Y, Hotate K. Automated suppression of polarization-fluctuation in resonator fiber optic gyro with twin 90° polarization-axis rotated splices[J]. Journal of Lightwave Technology, 2012, 31(3): 366-374.
- [13] Yu X H, Ma H L, Jin Z H. Improving thermal stability of a resonator fiber optic gyro employing a polarizing resonator[J]. Optics Express, 2013, 21(1): 358-369.
- [14] Liu H L, Wang W, Wang J J, et al. In-line polarizer used in all-0°-splice resonator fiber-optic gyro[J]. Applied Optics, 2013, 52(32): 7821-7825.
- [15] Dahlgren R P, Sutherland R E. Single-polarization fiber optic resonator for gyro applications[J]. Proceedings of SPIE, 1992, 1585: 128-135.
- [16] Ma H L, Chen Z, Jin Z H. Single-polarization coupler based on air-core photonic bandgap fibers and implications for resonant fiber optic gyro[J]. Journal of Lightwave Technology, 2014, 32(1): 46-54.
- [17] Jiao H C, Feng L S, Liu N, et al. Improvement of long-term stability of hollow-core photonic-crystal fiber optic gyro based on single-polarization resonator[J]. Optics Express, 2018, 26(7): 8645-8655.
- [18] Sanders G A, Taranta A A, Narayanan C, et al. Hollow-core resonator fiber optic gyroscope using nodeless anti-resonant fiber [J]. Optics Letters, 2020, 46(1): 46-49.
- [19] Shupe D M. Thermally induced nonreciprocity in the fiber-optic interferometer[J]. Applied Optics, 1980, 19(5): 654-655.
- [20] Liu J H, Liu Y F, Xu T H. Bias error and its thermal drift due to fiber birefringence in interferometric fiber-optic gyroscopes[J]. Optical Fiber Technology, 2020, 55: 102138.
- [21] Cao Y, Xu W Y, Lin B, et al. A method for temperature error compensation in fiber-optic gyroscope based on machine learning [J]. Optik, 2022, 256: 168765.

## Study on Polarization Error of Resonant Fiber Optical Gyroscopes in Varying Temperature Environments

Gao Tianxiang<sup>1</sup>, Li Jun<sup>2</sup>, Lan Shiqi<sup>2</sup>, Wu Fan<sup>2</sup>, Cheng Jun<sup>1</sup>, Qi Xinyuan<sup>1\*</sup>

<sup>1</sup>School of Physics, Northwest University, Xi'an 710127, Shaanxi, China;

<sup>2</sup>National Key Laboratory of Science and Technology on Aircraft Control, Flight Automatic Control Research Institute, Xi'an 710076, Shaanxi, China

### Abstract

**Objective** In response to the need for high-precision and engineering applications of resonant fiber optical gyroscopes (RFOGs), research is conducted on the relevant factors that affect polarization noises and thus the output error of gyroscopes in varying temperature environments. Polarization noise is one of the main optical noises that cause output errors in RFOGs. Since the core sensitive component of RFOGs, namely the fiber ring resonator (FRR), is mostly wound by polarization maintaining optical fiber, when the birefringence index of polarization maintaining optical fibers changes with temperature, it will cause the superposition and interference effects of the resonant light waves corresponding to the two intrinsic polarization states of the resonator, resulting in asymmetry in the resonance curve, polarization noises, and

detection errors at the resonance frequency point and thereby causing gyro output errors. Therefore, suppressing polarization noise in varying temperature environments has profound significance. The measures taken by researchers to suppress polarization noise can be divided into two categories: stabilizing the phase difference between primary and secondary polarization and reducing the intensity of secondary polarization states. Researchers have successively adopted a single 90° fusion joint scheme within the FRR, a twin 90° fusion polarization maintaining transmission FRR scheme, and a secondary polarization axis rotation fusion polarization starting resonant cavity to stabilize the primary and secondary polarization phase difference. Researchers have reduced the intensity of secondary polarization states by inserting polarization controllers, online polarizers, etc. into the FRR or utilized a new fiber optic scheme to reduce the impact of polarization noises on the gyroscope. The above studies have achieved good results in noise suppression, but most studies have been conducted at room temperature or small-range temperature variations. When facing engineering applications, gyroscopes need to improve their environmental adaptability within the full temperature range. To meet the needs of both high-precision and engineering applications, we study the factors that affect polarization noises and thus the output error of gyroscopes in varying temperature environments.

**Methods** Jones matrix is a relatively simple method to describe the polarization characteristics of optical devices. We establish a complete optical transmission model based on the Jones matrix method. By analyzing the clockwise and counterclockwise optical transmission in the resonant cavity, the difference between the coupling errors of the clockwise and counterclockwise polarization modes is used as the output error of the gyroscope, eliminating the common mode error, and the problem of using double the frequency deviation caused by polarization noise as the output error of the gyroscope in the past while ignoring the difference in forward and backward light transmission is solved. In the full temperature range of  $-40^{\circ}\text{C}$ – $80^{\circ}\text{C}$ , the factors that affect the polarization noise and lead to the gyro output error are simulated and calculated, including the angle alignment error of the coupler, the length difference of the optical fibers on both sides of the twin 90° fusion point, and the uneven temperature distribution difference of a section of optical fibers on the FRR or each adjacent end of optical fibers when the system is locally heated, so as to obtain the gap between the actual structure of the system and the theoretical calculation and quantify the control accuracy of relevant parameters based on specific gyro error requirements in varying temperature environments.

**Results and Discussions** First, based on the twin 90° fusion point integrated online polarizer structure, the resonant cavity optical path is modeled, and its polarization characteristics are analyzed to obtain the resonance curves of the clockwise and counterclockwise light transmission in the cavity for one cycle (Fig. 2). In addition, the frequency difference between clockwise and counterclockwise is taken as the output error of the gyroscope caused by polarization noises, and the influence of polarization errors on the gyroscope output under varying temperature environments is studied. When the ambient temperature changes within the whole temperature range, the errors caused by the polarization of clockwise and counterclockwise light transmission are very close, both within  $\pm 3^{\circ}/\text{h}$ , and the overall difference is within  $\pm 0.02^{\circ}/\text{h}$ , both showing periodic changes with temperatures (Fig. 3). However, this result cannot support the development requirements of the navigation level gyroscope engineering prototypes, and parameter control is needed to reduce the polarization error output. The relationship between the angle alignment error of the coupler (Fig. 4), the fiber length difference on both sides of the twin 90° fusion point (Fig. 5), and the output error of the gyroscope is simulated and calculated. Based on the control parameters obtained from this result and the gyro operating environment, active devices such as lasers or circuit components dissipate heat during normal operation, resulting in local temperature disturbance to the FRR close to them (Fig. 6), and the influence of the fiber ring temperature and its ambient temperature distribution difference on the gyro output error caused by polarization noise is analyzed, including the non-uniform temperature distribution difference on a section of optical fiber (Fig. 7) and the temperature distribution difference between two adjacent optical fibers (Fig. 8), which guides error distribution design due to polarization noise in varying temperature environments.

**Conclusions** We establish a complete optical transmission model for FRR based on the Jones matrix. By analyzing the polarization noise of the clockwise and counterclockwise optical transmission and adopting the dual point 90° fusion integrated online polarizer structure, the resonance curve in FRR is derived, and the gyroscope output caused by polarization error in varying temperature environments is obtained; due to the periodicity and regularity of the gyroscope output within the whole temperature range, the varying temperature range of  $-40^{\circ}\text{C}$ – $20^{\circ}\text{C}$  is used instead of the full temperature environment, and different influencing factors are analyzed separately. The results show that when the

extinction ratio of the online polarizer is 30 dB, the alignment error of the coupler angle is less than  $2.78^\circ$ , and the output error of the gyroscope is less than  $0.01(^{\circ})/\text{h}$ ; as the coupler coefficient  $k$  gets larger, the fault tolerance value of the fiber length difference on both sides of the double  $90^\circ$  fusion point becomes higher. When  $k$  is 0.05, and  $\Delta L$  is controlled within 0.207 m, there is a gyroscope output error of less than  $0.01(^{\circ})/\text{h}$ . On this basis, when the temperature distribution on a section of optical fiber is uneven due to the internal temperature rise of the gyro prototype in engineering applications, the difference of the uneven temperature distribution should be less than  $13.2\ ^\circ\text{C}$ ; when there is a non-uniform temperature difference between every two adjacent fibers on the FRR, its value should be less than  $3.122\ ^\circ\text{C}$ , and the output error of the gyroscope is less than  $0.01(^{\circ})/\text{h}$ . The above analysis is based on the requirements of suppressing polarization noises in gyroscopes, which provides certain theoretical guidance for error allocation design in full-temperature environments.

**Key words** resonant fiber optical gyroscope; Jones matrix; polarization noise; varying temperature environment